RADIO-MICROLENSING IN B1600+434: PROBING MACHOs AT HIGH-REDSHIFTS

L.V.E. Koopmans[1,2,3], A.G. de Bruyn[4,1], J. Wambsganss[5,6], C.D. Fassnacht[7],R.D. Blandford[3]
[1]*Kapteyn Astronomical Institute, P.O.Box 800, NL-9700 AV Groningen, The Netherlands*
[2]*Jodrell Bank Observatory, Lower Withington, Macclesfield, Cheshire SK11 9DL, UK*
[3]*Caltech, Mail Code 130-33, Pasadena CA 91125, USA*
[4]*NFRA-ASTRON, P.O.Box 2, NL-7990 AA Dwingeloo, The Netherlands*
[5]*University of Potsdam, Institute for Physics, Am Neuen Palais 10, 14469 Potsdam, Germany*
[6]*MPI für Gravitationsphysik, "Albert-Einstein-Institut", Am Mühlenberg 1, 14476 Golm, Germany*
[7]*NRAO, P.O.Box 0, Socorro, NM 87801, USA*

We shortly review the evidence for the detection of *radio-microlensing* in the CLASS gravitational lens system B1600+434. We then present some of the latest results from our multi-frequency monitoring campaign and compare these observations with preliminary results from new Extreme-Scattering-Event (ESE) and radio-microlensing simulations.

1 Introduction

There is growing evidence that the lensed images of the CLASS[a] gravitational lens system B1600+434 (Jackson et al. 1995; Jaunsen & Hjorth 1997; Koopmans, de Bruyn & Jackson 1998) show strong non-intrinsic (i.e. 'external') flux-density variations, when observed at radio wavelengths (Koopmans et al. 2000a). A detailed analysis of 8.5–GHz lightcurves of B1600+434 obtained during a 1998 VLA monitoring campaign showed that these external flux-density variations are most likely caused by μas-scale relativistic subcomponents in the lensed source, which are being microlensed by massive compact objects in the dark-matter halo around the lensing galaxy at z=0.41 (Koopmans & de Bruyn 2000). The most likely alternative explanation, i.e. Galactic scintillation, was shown to implausible, based on a number of arguments (see Koopmans & de Bruyn 2000; Koopmans et al. 2000b). An optical monitoring campaign with the Nordic Optical Telescope (NOT) in 1998-1999 has shown evidence for the presence of optical microlensing in B1600+434 (Burud et al. 2000) as well, although it is not yet clear which of two lensed images (or both) undergo microlensing.

In Sect.2 we present some of the latest results from our 1999-2000 multi-frequency VLA observations of B1600+434. In Sect.3.1, we focus on a second alternative explanation (besides scintillation) for the external radio variability, i.e. Extreme Scattering Events (ESE). In Sect.3.2, we report on some very preliminary results from new *radio-microlensing* simulations for B1600+434. In Sect.4, we summarize our results.

2 Multi-Frequency VLA Observations of B1600+434

In 1999 a new VLA monitoring campaign of B1600+434 in A- and B-array was started at 1.4, 5 and 8.5 GHz (e.g. Koopmans et al. 2000b). We chose to observe over a wide frequency range, because it enables us to disentangle different sources of external variability, such as microlensing and scintillation (Koopmans & de Bruyn 2000). Here, we will *only* report on some preliminary results of the 5–GHz observations. The light curves of the the lensed images of B1600+434 are shown in Fig.1.

The 5–GHz lightcurve of image A, which predominantly passes through the dark-matter halo of the edge-on spiral lens galaxy, shows strong external variations, continuing the behavior

[a]Cosmic Lens All Sky Survey

00

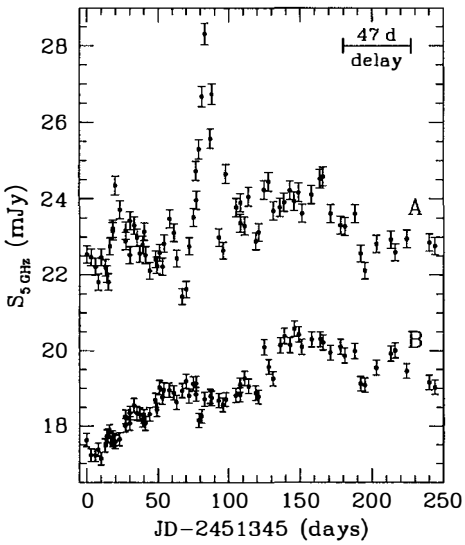

Figure 1: Preliminary results (at 5 GHz) from the 1999/2000 VLA monitoring campaign of B1600+434. The upper light curve (image A) passes through the dark-matter halo of the edge-on spiral lens galaxy. Note several strong (up to 30%) events in the upper lightcurve and the complete absence of these events in the lower light curve (image B) after the time delay of ∼47 days.

already seen in the 1998 VLA 8.5–GHz lightcurves (Koopmans & de Bruyn 2000). In 1998 and again in 1999-2000, the lightcurve of image B shows much less short-term variability during the monitoring campaign. In this proceeding we will *only* focus on the strongest 5-GHz event that starts around day 67 (Fig.1). A ∼30% increase in the flux-density is seen with a maximum around day 83. After that an almost similar decrease in flux-density is observed, reaching a minimum around day 96. This comparatively well-sampled ∼1–month event is not detected in the other lensed image after the time delay of about 47 days (Koopmans et al. 2000a; see also Burud et al. 2000) and must therefore be of external origin. The VLA 8.5-GHz lightcurve of image A simultaneously shows the same external event with almost comparable amplitude. At 1.4 GHz the event is not detected.

3 Observations versus Simulations

3.1 Extreme Scattering Events: Can they explain what we see in B1600+434?

ESEs are strong non-intrinsic variations in the lightcurves of compact extra-galactic radio sources and pulsars, first discovered by Fiedler et al. (1987). ESEs can typically be characterized by a strong decrease (up to 50% in some cases) in the source flux-density at low frequencies (∼2 GHz) during a period of several weeks to months (e.g. Fiedler et al. 1994). In most ESEs almost no variations are seen at higher frequencies (∼8 GHz), with the exception of 0954+658 (Fiedler et al. 1987, 1994). The most plausible explanation of these events is that a plasma cloud with high electron density moves across the line-of-sight to the source, causing strong refractive (de)focusing (Romani, Blandford & Cordes 1987) and/or stochastic broadening (Fiedler et al. 1987, 1994), resulting in observable flux-density variations.

We have have examined the strongest event seen at 5 GHz (Fig.1) in terms of the refractive (de)focusing model. The stochastic-broadening model — which can be understood in terms of a source convolution with a space-varying kernel (Fiedler et al. 1994) — has great difficulties in explaining 'caustic-type' *increases* in flux-density, which have been observed in for example 0954+658. We therefore use the simple refractive (de)focusing model model from Clegg, Fey

& Lazio (1998), who describe the plasma cloud as a Gaussian over- or underdensity. We have examined other models as well, but the precise details of the model do not alter the main conclusions. In Fig.2a, we have shown the results from one of the models that gives a fairly good representation of the observed event seen in Fig.1. The model gives a similar event at 8.5 GHz and almost no variations at 1.4 GHz, as has been observed. However, at 5 GHz the model requires a negative lens strength $\alpha \approx -0.2$, where $\alpha = 3.6\lambda^2 \Delta N_0 D\, a^{-2}$, λ is the radio-wavelength in cm, ΔN_0 is the central electron surface-density contrast of the cloud in units of cm^{-3} pc, D is the cloud distance in kpc (for a source at infinity) and a is the cloud size in units of AU (see Clegg et al. 1998 for more details). For the model in Fig.2a, we require a source size at 5 GHz equal to $\beta \approx 1.0$ times the cloud size. We assume that the source size grows linearly with λ. Changing α and/or β only slighty from these values quickly results in a very poor comparison with the lightcurves of at least one of the frequencies. No solutions for positive α have been found, independent of the precise model for the electron surface density. The result is therefore quite robust. However, because $\alpha < 0$, one immediately notices that $\Delta N_0 < 0$. In other words, one requires a considerable electron *underdensity* of the 'cloud' (i.e. 'bubble') compared to its immediate surroundings. Filling in some typical numbers of genuine ESEs ($D \approx 0.5$ kpc, $a \approx 1$ AU; e.g. Fiedler et al. 1994) and taking λ=6 cm, we find $\Delta N_0 = -3 \cdot 10^{-3}$ cm^{-3} pc. If we assume the 'bubble' is spherical, the central electron underdensity is $\Delta n_0 \approx -10^3$ cm^{-3}, which is a more than 10^3 times the typical electron density in the Galactic ISM. Consequently, the surrounding of this 'bubble' must have a similar electron *overdensity*. If the electron temperature inside the 'bubble' is about $T_e = 10^4$ K, it would collapse within about 2 weeks. This time scale is smaller than the event duration of $\sim$1 month. Reducing a by a factor of say 10 would still require $\Delta n_0 \approx -10^2$ cm^{-3}, but more seriously it reduces the collapse time to only several days.

All in all, it appears unlikely that the observed event (Fig.1) can be a genuine ESE. It (i) does not resemble any other ESE (see Fiedler et al. 1994), (ii) requires a severely localized electron *underdensity* and consequently a similar electron overdensity around it, and (iii) it is difficult to see how such a 'bubble' could be generated and remain stable for a considerable period of time (i.e. several weeks).

3.2 Radio Microlensing

In Koopmans & de Bruyn (2000), the VLA 8.5-GHz light curves were compared with microlensing simulations. Because of the absence of a distinct isolated microlensing events in the lightcurves, several assumptions had to be made in deriving properties of the compact objects in the halo and the source structure. The strong events in the 1999/2000 VLA light curves (Fig.1) allows us to improve this analysis and do a comparable study as for Q0957+561 (e.g. Schmidt & Wambsganss 1998; Refsdal et al. 2000). We have generated microlensing magnification patterns on grids of 4096×4096 pixels, having sidelengths of 409.6 Einstein radii. We generate a number of magnification patterns, taking $\kappa = \gamma = 0.2$ for the image (A) passing through the dark-matter halo (e.g. Koopmans et al. 1998), for different fractions of the surface density composed of compact objects (f_c=10%, 30% and 100%) and different sizes for the relativistic subcomponents. We then simulate $\sim 10^5$ lightcurves for a range of relativistic-subcomponent velocities and for each combination of f_c and source size. The analysis of these lightcurve and the comparison with the observations is still work in progress. A not uncommon example of one of the light curves, however, is shown in Fig.2b for f_c=30% and a component size of 0.5 Einstein radius. For a subcomponent containing 10% of the total source flux-density, this event would correspond to a $\sim$30% event in the light curve of image A, comparable to the event in Fig.1.

02

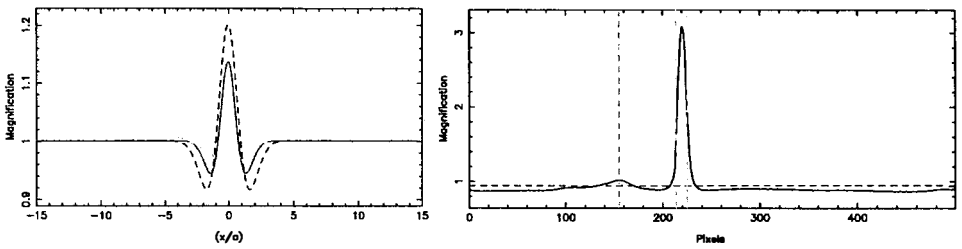

Figure 2: **Left:** ESE simulation of the strongest 'external' event shown in Fig.1. The light curves are for 8.5 GHz (solid), 5 GHz (dash) and 1.4 GHz (dot-dash). **Right:** A microlensing simulation. The horizontal dashed line gives the average of the light curve. The two close vertical dashed lines indicate the FWHM of the strongest event. The other vertical dashed line indicates the second strongest event. See Sections 3.1–2 for more details about these models.

4 Conclusions

We find that ESEs can only explain the strongest non-intrisic 5-GHz variation in lensed image A of B1600+434 (Fig.1), if the Galactic ionized ISM contains ~1–AU sized regions that have electron densities differing by $\Delta n_0 \approx -1000$ cm^{-3} from their immediate surrounding. Not only have these type of flux-density variations never been seen before in (unlensed) radio sources, but the hypothesised plasma structures responsible are unlikely to be stable for longer than several weeks. We are currently investigating even more 'exotic' plasma models. Preliminary microlensing simulations show that the flux-density variations as seen in B1600+434 *can* occur quite regularly *if* the lensed source contains relativistic sub-components with a size similar to the Einstein radius of the compact objects, even if the surface density of massive compact objects in the lens galaxy is much lower than the critical surface density. More complete data, ESE and microlensing analyses will be given in several forthcoming papers.

References

1. Burud, et al. 2000, astro-ph/0007136
2. Clegg, Fey & Lazio, 1998, ApJ 496, 253
3. Fiedler, Dennison, Johnston & Hewish, 1987, Nature 326, 675
4. Fiedler, Dennison, Johnston, Waltman, & Simon, 1994, ApJ 430, 581
5. Jackson et al. 1995, MNRAS 274, L25
6. Jaunsen & Hjorth, 1997, A&A 317, L39
7. Koopmans, de Bruyn, & Jackson, 1998, MNRAS 295, 534
8. Koopmans, de Bruyn, Xanthopoulos, & Fassnacht, 2000a, ApJ 356, 391
9. Koopmans, de Bruyn, Wambsganss, Fassnacht, 2000b, astro-ph/0004285
10. Koopmans & de Bruyn, 2000, A&A 358, 793
11. Refsdal, Stabell, Pelt, Schild, 2000, astro-ph/0005371
12. Romani, Blandford & Cordes, 1987, Nature 328, 324
13. Schmidt & Wambsganss, 1998, A&A 335, 379